



The Effect of Bonding Time on Dissimilar Joint Properties Between Inconel 625 and AISI 316L Using Transient Liquid Phase Bonding Method with Cu Interlayer

Mehrdad Ajabshiri, Morteza Shamanian, Ali Ashrafi, and Mohammad Ali Karimi

Submitted: 18 June 2021 / Revised: 22 September 2021 / Accepted 26 October 2021 / Published online: 24 January 2022

In this paper, the effect of bonding time on the microstructural and mechanical properties of a dissimilar joint between Inconel 625 and AISI 316L was investigated using a Cu interlayer. For this purpose, the bonding was performed at the bonding temperature of 1100 °C for 15, 30 and 60 minutes. Field emission scanning electron microscope equipped with energy-dispersive x-ray spectroscopy was used for microstructural analysis. X-ray diffraction was used to identify the formed phases in the different zones of joint bonding. Shear strength and hardness tests were performed to evaluate the mechanical properties of the joints. Microstructural observations showed that the interface of Inconel 625 with the Cu interlayer contained Mo- and Nb-rich MC type carbide. Also, microstructural investigations showed that the bonding zone contains (Ni, Cr, Fe)-rich nanosized deposits in the Cu matrix. The specimen bonded at 1100 °C for 30 minutes demonstrated the maximum shear strength of 470 MPa, and its fractography dominantly showed a ductile dimple fracture. The isothermal solidification of Cu showed that the TLP bonding is controlled by both the diffusion kinetics and diffusion thermodynamics in the solidification of Cu. The asymmetric diffusion of Cu into the base metals caused the bonding interface shifts to 316L side.

Keywords bonding time, Cu interlayer, inconel 625, transient liquid phase

1. Introduction

Inconel 625 superalloy has attracted industry and researchers' attention due to its remarkable mechanical properties and excellent corrosion resistance at very high temperatures. This alloy has been used in the reactor core of nuclear power plants, boilers, piping, chemical tank impellers, turbine blades of power plants and aerospace engine components (Ref 1, 2). Due to the high cost of the Inconel 625 alloy, this alloy's dissimilar joints are used in most industries. For example, the dissimilar joint of the Inconel 625 and AISI 316L has been used by NASA to construct small-scale boilers and reactors for high-temperature chemical processes, especially the process of calcination of diluted chromic acid (Ref 3, 4). Researchers have investigated the bonding of Inconel 625 alloy to AISI 316L by various fusion welding methods such as gas tungsten arc welding (GTAW) (Ref 5), laser beam welding (LBW) (Ref 6) and electron beam welding (EBW) (Ref 7). These studies on fusion bonding methods had aimed to control detrimental phases, and the results had been somewhat effective in selecting suitable fillers as well as controlling welding variables. However, the problem of detrimental phases remains (Ref 8). Researchers have suggested that one solution for this problem

is solid-state bonding. The transient liquid phase (TLP) bonding has been significantly improved for the bonding of dissimilar metals, especially superalloys. The TLP bonding process is performed by a filler metals which have melting point depressant (MPD) elements (Ref 9, 10) or form a eutectic compound with elements of base materials (Ref 11, 12). In filler metals containing MPD elements, isothermal solidification is based on the diffusion of MPD elements from interlayer to base materials and vice versa. By diffusion of MPD elements, the melting point of filler metal increased, leading to solidification of molten interlayer at constant temperature (Ref 13). With continuous diffusion of MPD element from the liquid to the base metal, the volume of liquid kept at equilibrium decreases, causing solidification front to advance toward the joint center. If sufficient time is not provided for isothermal solidification at the joint temperature, the formation of eutectic microstructures and intermetallic compounds along the joint might occur (Ref 14). Several researchers have investigated the TLP bonding of Inconel 625 (Ref 15-17). In these studies, AWS BNi-2 filler metal was used as an interlayer for bonding. The presence of boron in the interlayer causes the formation of eutectic phases and intermetallic compounds that affect the final bonding properties and reduce the mechanical properties and corrosion resistance (Ref 17, 18).

Alireza Doroudi et al. (Ref 17) investigated the TLP bonding of Inconel 625 superalloy using AWS BNi-2 (Ni-3Fe-3.1B-4.5Si-7Cr) filler metal at 1025 °C for 35, 65 and 95 minutes. Their research showed that by increasing the bonding time, the diffusion of the MPD element from the bonding zone increases, and the isothermal solidification is completed in 95 minutes. They reported a maximum joint shear strength of 448 MPa. In a study by Wen-Shiang Chen et al. (Ref [19]), TLP bonding of Inconel 625 with Cu interlayer was examined at 1120, 1140, 1160, 1180 and 1200 °C for 10, 30 and 60 minutes, respectively. In this study, gray deposits were observed in the

Mehrdad Ajabshiri, Morteza Shamanian, Ali Ashrafi, and Mohammad Ali Karimi, Department of Materials Engineering, Isfahan University of Technology, 84156-83111 Isfahan, Iran. Contact e-mail: mehrdad.ajabshiri@gmail.com.

Cu matrix, identified as CrNi₃ compounds using transmission electron microscopy. In this joint, the maximum shear strength of 470 MPa was achieved at a temperature of 1160 °C for 60 minutes. Their results showed that by increasing the bonding temperature or bonding time, especially after the bonding temperature of 1160 °C, the Cu/Ni-rich matrix gradually undergoes solidification shrinkage and forming shrinkage voids at the joint. Because the dissolution of the Inconel 625 substrate in the molten Cu interlayer during the TLP bonding process increases with increasing temperature or bonding time, the Cu/Ni-rich substrate in the bonding zone gradually shrinks with increasing temperature or bonding time. Isothermal solidification of the melt in the interlayer can lead to the formation of solidification shrinkage voids. The coalescence of these microvoids, especially at the bonding temperature of 1200 °C, strongly affects the joint's shear strength and reduces the strength to less than 260 MPa. In a study by Khan et al. (Ref 20), the 2205 micro-duplex stainless steel (Fe-22 Cr-3 Mo-5.5 Ni-0.17 N) bonding was investigated using a pure Cu interlayer and a foil based on the Fe-B-Si system. The results showed that the bonding made with the Fe-B-Si interlayer forms a ferritic structure in the bonding zone. By increasing the bonding time, the Widmanstätten austenitic phase structure is formed within the bonding zone. Bonding with Cu interlayer showed more microstructural homogeneity with the base metal alloy structure by increasing bonding time. In a study conducted by Ghasemi et al. (Ref 21), the competition between the kinetics and thermodynamics of diffusion in the TLP bonding of Monel 400 alloy (Ni-33.56Cu-1.88Fe-0.98Mn-0.13C-0.12Si) was investigated using two different filler metals, including pure Cu and Ni-Si-B. Interestingly, faster isothermal solidification was observed in bonding with the Cu filler metal. Despite the lower diffusion of Cu as a substitute MPD element in Ni-based alloys compared to boron as an interstitial MPD element, its higher solid solubility in the Monel 400 provides a greater thermodynamic driving force for isothermal solidification.

Given that no research has been done on the TLP bonding of IN 625/AISI 316L so far, the purpose of this paper is to investigate the dissimilar bonding behavior of IN 625/AISI 316L using a TLP bonding process with a pure Cu interlayer.

2. Experimental Work

In this study, the samples were made of Inconel 625 alloy and AISI 316L stainless steel hot rolled plates with the dimensions of 40×15×5 mm. Table 1 shows the chemical compositions of the base metals used in this study as determined by a Quantometer model ARUN. Pure Cu with a thickness of 30 μm was applied as coating on AISI 316L to join the base metals with the Cu interlayer. For this purpose, the substrates were ground by 400 to 1200 grit SiC paper and polished by 6μm diamond paste. Because only one substrate

surface is considered, the rest of the surfaces are covered with varnish to prevent Cu coating formation. The substrate was then kept in a sodium hydroxide solution (NaOH 10 wt.%) at 70 °C for 15 minutes for degreasing and rinsed with distilled water. Finally, the substrate was immersed for 1 minute in a solution of hydrochloric acid (HCl 10 vol. %), and samples were immediately transferred to a coating bath. Stainless steel samples were used as cathodes, and Cu sheets with 99% purity were used as anodes. The composition and conditions of the Cu sulfate plating bath are presented in Table 2. Coated samples of AISI 316L stainless steel and Inconel 625 superalloy were degreased using acetone in an ultrasonic bath and then placed on top of each other in order to perform the bonding process. The resulting set was placed between the fixture plates made of St37 steel, and a constant load with a pressure of 0.5MPa was applied. The samples were then placed in a vacuum furnace with a 5×10⁻⁵ torr pressure. The bonding process was performed at the bonding temperature of 1100°C at three different durations of 15, 30 and 60 minutes. The bonded specimens were examined for microstructural studies, diffusion layer measurement and bond uniformity control using a field emission scanning electron microscope (FESEM) model QUANTA FEG-450 equipped with energy-dispersive x-ray spectroscopy (EDS). For this purpose, the cross section of specimens was grounded with 240 to 2400 SiC grit paper and finally polished by 0.05 alumina particle suspension. For etching, the Cu and AISI 316L side, a solution of 2gr FeCl₃, 24mL H₂O and 6mL HCl solution was used. A solution containing 33% hydrochloric acid, 33% nitric acid and 34% distilled water was used for 15 seconds to etch the Inconel 625 side. To identify the formed phases using XRD in different areas of the bonding, the bonded samples were cut using an electric discharge machine (EDM) according to Fig. 1. The XRD analysis was performed by x-ray diffractometer (model PhilipsPW1730) with Cu Ka radiation at scan rate of 1°/min and scan step of 0.05°. The microhardness test was performed to measure the joint hardness characteristics using a Clark LM-100AT hardness tester with a load of 100g for 10 seconds. The shear test was performed to determine the shear strength with a type 10-ton Wolpert strength test machine, model FM2750, with a 0.5 mm/min crosshead speed.

Table 2 Composition and conditions of copper sulfate plating bath

Cu ₂ SO ₄ (gr/l)	150
H ₂ SO ₄ (gr/l)	30
Temperature (°C)	25
Agitation (rpm)	400
Cathodic current density (A/dm ²)	2
Time (minute)	30
PH	0.5

Table 1 Chemical composition (wt.%) of bonded base metals

Element	Ni	Cr	Fe	Mo	Nb	C	Mn	Si	P	S	Al	Ti	Co	N
Inconel 625	Bal.	22.76	4.18	7.96	3.6	0.03	0.2	0.37	0.01	0.01	0.36	0.39	1	...
316L	10.12	16.7	Bal.	2.38	...	0.02	1.68	0.51	0.04	0.03	0.06

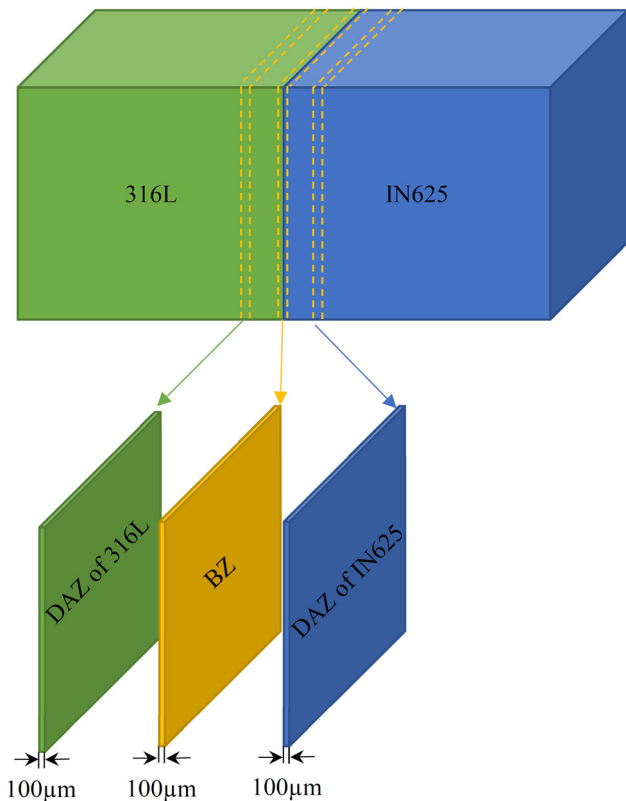


Fig 1. The schematic of the extracted specimens from the different zones of the TLP bonded specimen for XRD test

3. Results and Discussion

3.1 Microstructural Characterization

Figure 2 shows an electron microscopy image of the bonding section of the Inconel 625 to AISI 316L with Cu interlayer at the bonding temperature of 1100 °C for 15 minutes. During the TLP bonding process, the Cu melts in the interlayer. Therefore, parts of the Inconel 625 and AISI 316L in contact with the molten interlayer are separated from the base metal and dissolved in the interlayer. At this stage, the molten Cu is not in thermodynamic equilibrium with the base metals. Cu atoms must diffuse into the base metals to maintain thermodynamic equilibrium, and reciprocally, the base metal atoms will diffuse into the molten Cu region. According to the binary phase diagrams of Cu-Ni and Cu-Fe, Cu and Ni are entirely soluble, but Cu and Fe are not highly soluble (Ref 22). Therefore, a more significant part of Inconel 625 than AISI 316L will dissolve into the bonding zone. Figure 3 shows the EDS analysis results of different points marked in Fig. 2. The diffusion of Cu in the Inconel 625 side (Point B) was much greater than the diffusion of Cu in the stainless steel side (Point A). The diffusion of Ni from Inconel 625 and the diffusion of

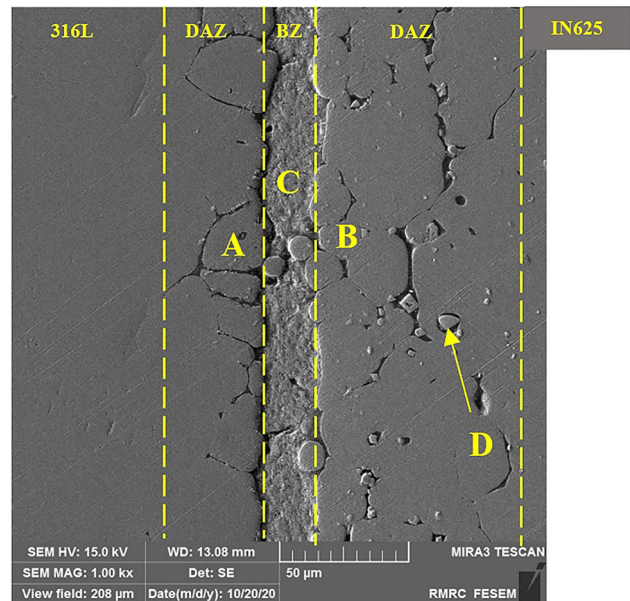


Fig 2. FESEM image of the IN 625/Cu/AISI 316L joint made at the bonding temperature of 1100 °C for 15 minutes

Fe from stainless steel into the Cu interlayer are also significant (Point C). Dissolution of Inconel 625 causes the entry of Ni, Mo and Nb elements into the molten Cu. Due to the diffusion of Ni into the Cu interlayer, the solubility of Mo and Nb in the Inconel 625 is reduced, resulting in the formation of MC type carbide rich in Mo and Nb in the interface (Point D).

Inconel 625 contains chemical elements having a high affinity for carbon, such as Mo and Nb. For this reason, the diffusion of carbon can result in formation of carbides in the DAZ of Inconel 625. Isothermal transformation diagram of Inconel 625 shows that the parameters of the TLP bonding are close to the carbide formation area, especially MC types (Ref 23). As the temperature rises above 1050°C, the carbides dissolve in the matrix of Inconel 625 and the amount of carbon in the matrix increases. In the DAZ of Inconel 625, with the diffusion of Ni to the Cu interlayer and reciprocally the diffusion of Cu to DAZ of Inconel 625, the concentration of Cu in DAZ of Inconel 625 increases and the concentration of Ni in the DAZ of Inconel 625 decreases. As a result, the solubility of Mo and Nb in the DAZ of Inconel 625 decreases, which form carbide with carbon.

According to Fig. 2, three regions in the TLP joint section of IN 625/Cu/AISI 316L can be detected:

- (1) Area related to AISI 316L and Inconel 625 base metals.
- (2) Cu Diffusion Affected Zone (DAZ).
- (3) Bonding Zone (BZ).

Grain boundary liquation on the AISI 316L stainless steel side and the formation of MC carbides rich in Mo and Nb on

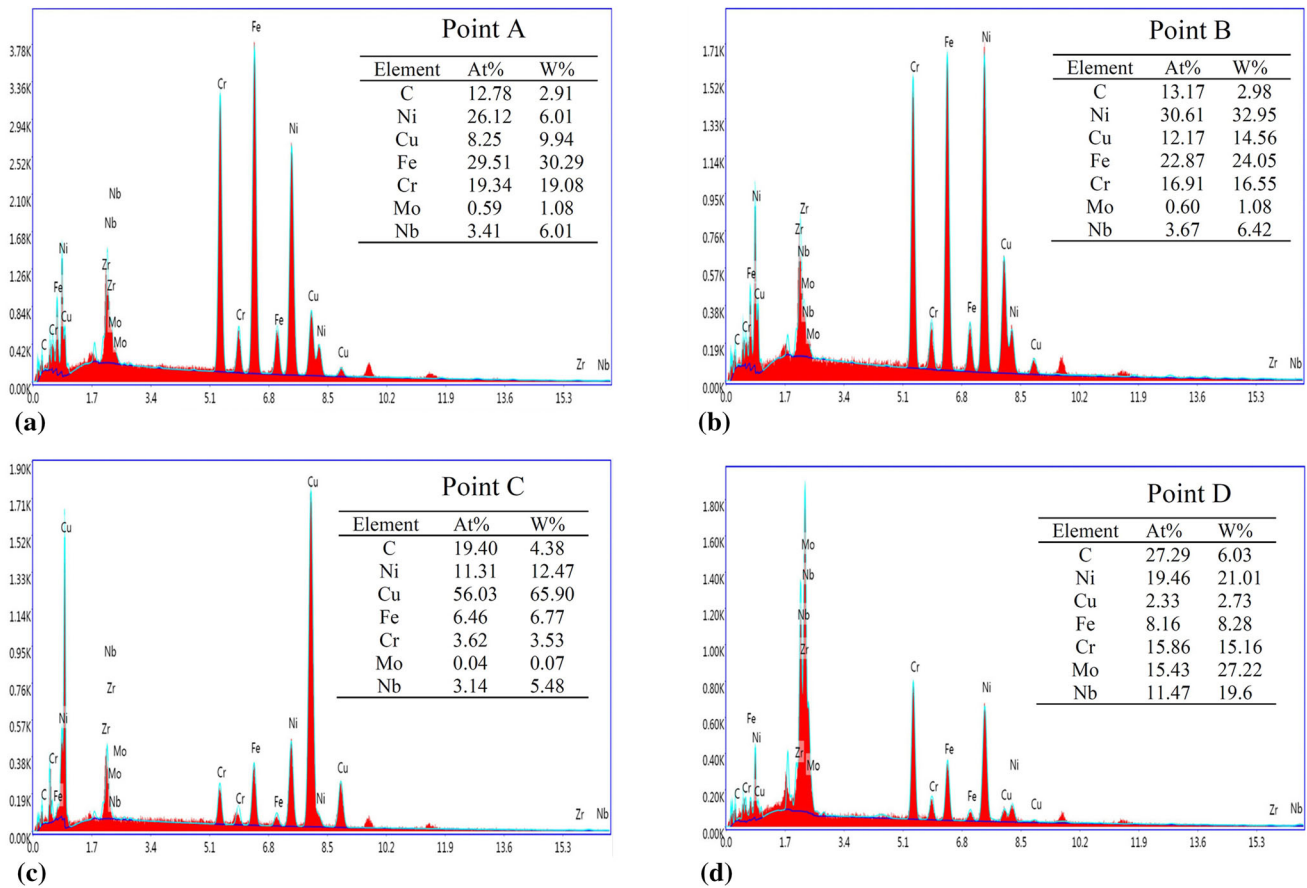
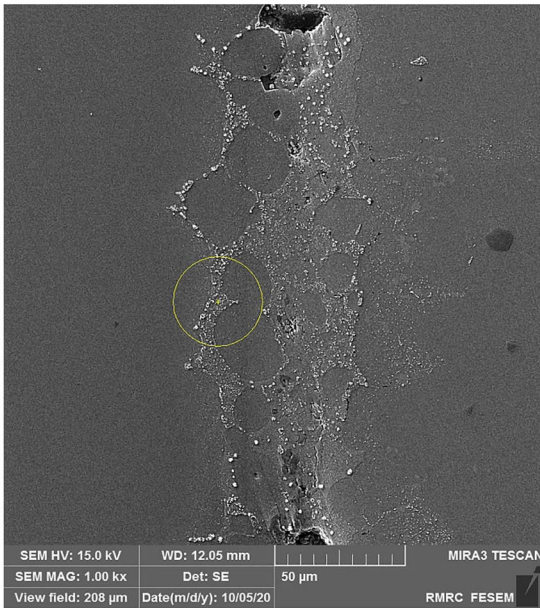


Fig 3. EDS analysis of points marked in Fig. 2

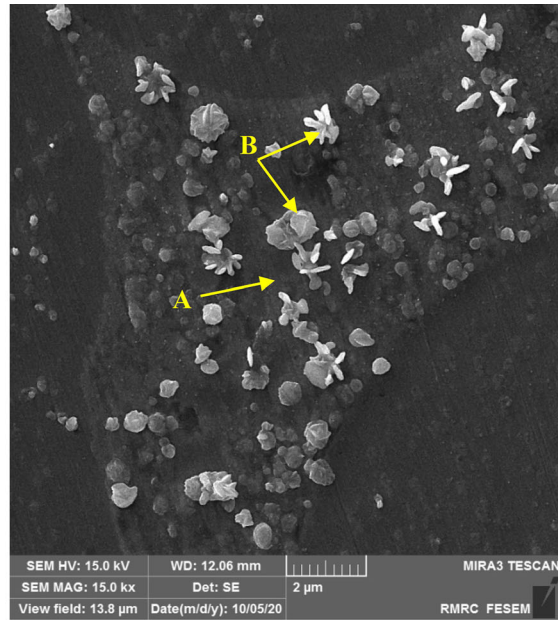
the Inconel 625 side are characteristics of the DAZ. As shown in Fig. 2, in the BZ, precipitations are visible in the Cu matrix, which can be observed only in the polished state and without etching with a FESEM microscope. Figure 4 shows electron microscopy images and the EDS results of precipitations in IN625/Cu/316L bonding at 1100 °C for 30 minutes in polished and non-etched state. Figure 5 also displays an elemental mapping analysis of the BZ containing these precipitations. According to EDS results and mapping analysis it is evident that these precipitations are Ni-, Cr- and Fe-rich. Since Cr and Fe are insoluble in Cu, they can form precipitates in the Cu matrix during the cooling stage. Figure 6 shows the microstructure of the samples made at the bonding temperature of 1100 °C for 15, 30 and 60 minutes. According to Fig. 6, it can be seen that by increasing the bonding time and diffusion of Cu into base materials, the width of the BZ has decreased, resulting in the establishment of a complete joint between the two base metals in some areas. The disappearance of the Cu from the BZ confirms that a binding time of 60 minutes is sufficient to complete the isothermal solidification (Fig. 6(c)) (Ref 24). Also, in Fig. 6(c), the displacement of the bonding interface toward the 316L base metals is significant. This is due to that the diffusion rate of Cu into the Inconel 625 is much more than

that of the Cu diffusion rate into the 316L base metal. Figure 7 shows the XRD test results of the different zones in the joint bonding at the 1100 for 30 minutes. XRD diffraction patterns of 316L and Inconel 625 base metals show the austenite (γ) phase (Fig. 7a and e). In the interlayer, intense peaks at 43.62°, 50.81° and 74.58° assigned to the austenite (γ) phase (Fig. 7c). On the other hand, the diffusion of Nb from the Inconel 625 to the Cu interlayer and the 316L stainless steel side has caused the formation of NbC carbide in the interlayer (Fig. 7c) and the DAZ of 316L stainless steel (Fig. 7b). Peaks at 44.75° and 64.93° in the DAZ of 316L side (Fig. 7b) assigned to ferrite phase, which indicates that the delta ferrite phase has increased during the TLP bonding. Also, the peak at 78.26° in DAZ of 316L (Fig. 7b) correspond to the $Cr_{23}C_6$ carbides that have formed during the TLP in the cooling stage.

Figure 8 also shows the Cu, Ni and Fe concentration distribution across the joint made at the bonding temperate of 1100 °C for bonding times of 15, 30 and 60 minutes. According to Fig. 8(a), it can be seen that with increasing the bonding time from 15 to 30 minutes the Cu diffusion on both the AISI 316L and the Inconel 625 sides has increased while with increasing the bonding time from 30 to 60 minutes the Cu diffusion toward base metals decreases. This procedure is



(a)



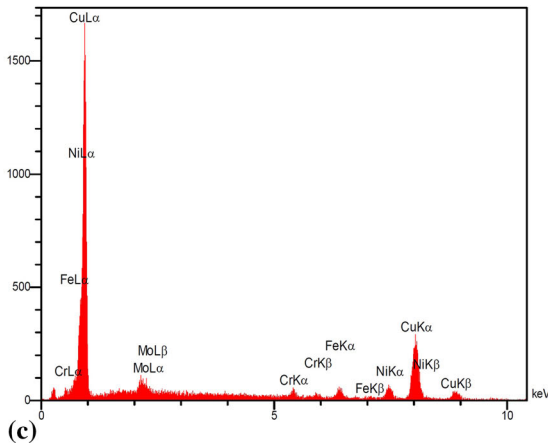
(b)

Point A

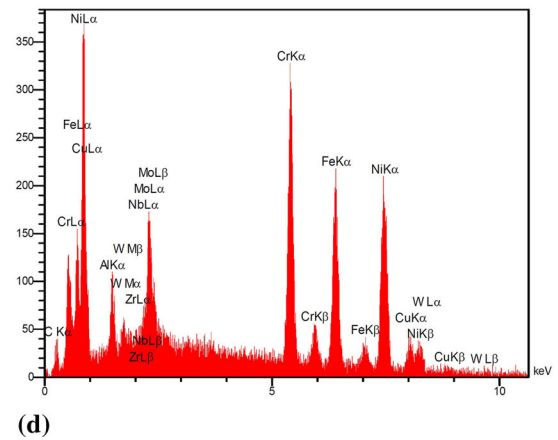
Element	At%	W%
Cr	1.7	2.08
Fe	3.74	4.24
Ni	9.67	10.47
Cu	80.34	80.21
Mo	3.0	4.53

Point B

Element	At%	W%
C	27.60	7.27
Cr	18.55	20.96
Fe	17.34	20.96
Ni	28.74	36.98
Cu	4.35	6.10
Mo	3.0	6.89
Nb	0.42	0.84



(c)



(d)

Fig 4. FESEM images of precipitations formed in the Cu matrix at IN 625/Cu/AISI 316L joint made at the bonding temperature of 1100 °C for 30 minutes

repeated for the diffusion of Ni from Inconel 625 and the diffusion of Fe from the 316L stainless steel side, like the diffusion of Cu (Fig. 8b, c). These findings mean that the diffusion of Cu, Fe and Ni elements, in addition to temperature and time of bonding, is also dependent on the grain size of the base metal. Table 3 shows the grain size and average grain diameter of 316L stainless steel at different bonding times.

Although the diffusion of Cu into base metals increases by increasing the bonding time but, this increase in diffusion is affected by the microstructure of the base metals. One of the preferred places for Cu to diffuse is the grain boundary of the base metal. Researches showed that by increasing the bonding temperature or holding time in the Inconel 625 and the AISI 316L stainless steel at temperatures above 1050 °C, significant

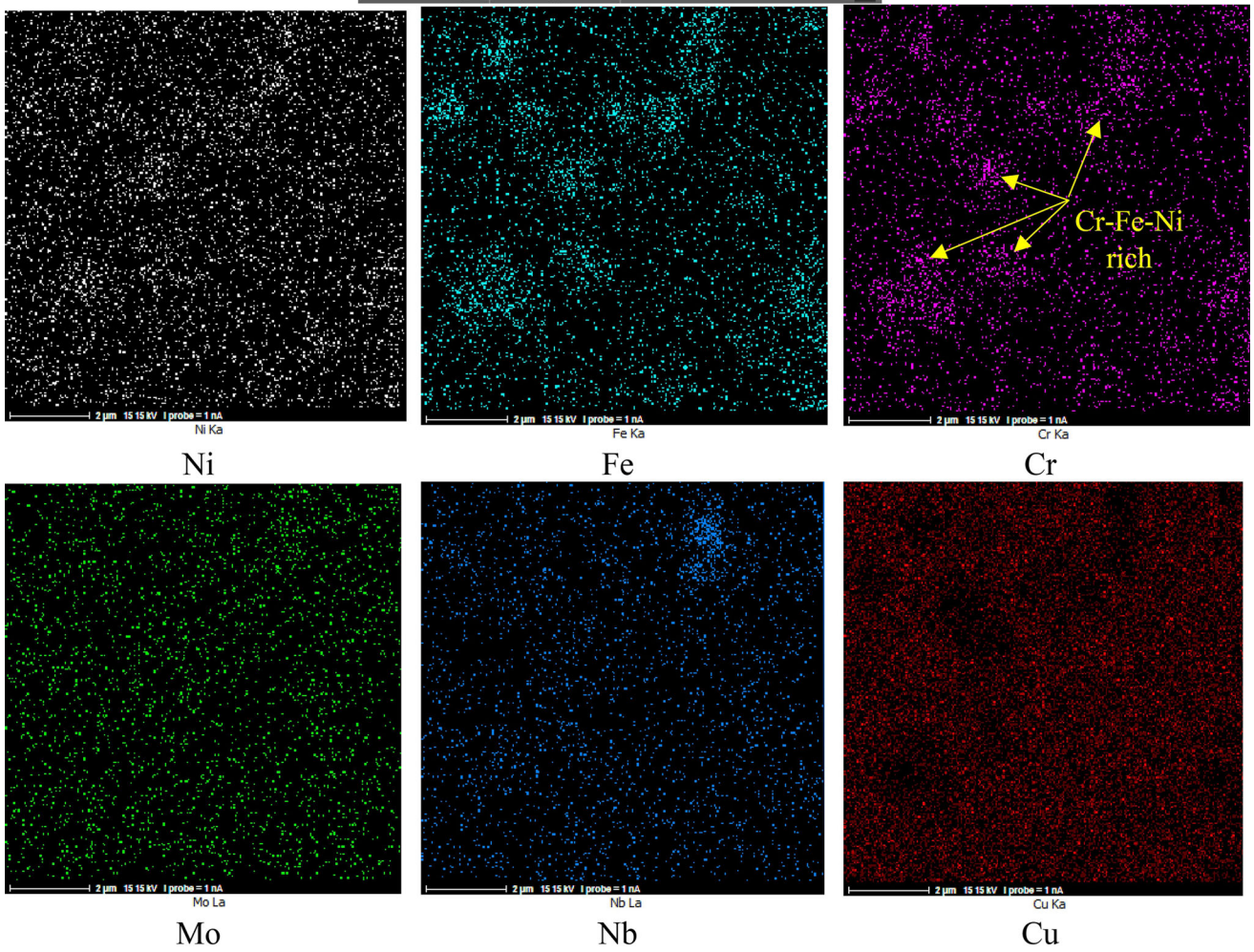
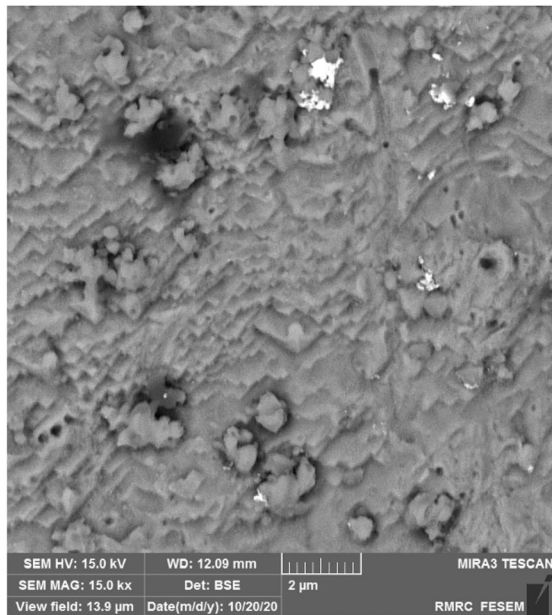


Fig 5. Elemental mapping analysis of the bonding zone in the IN 625/Cu/AISI 316L joint made at the bonding temperature of 1100 °C for 30 minutes

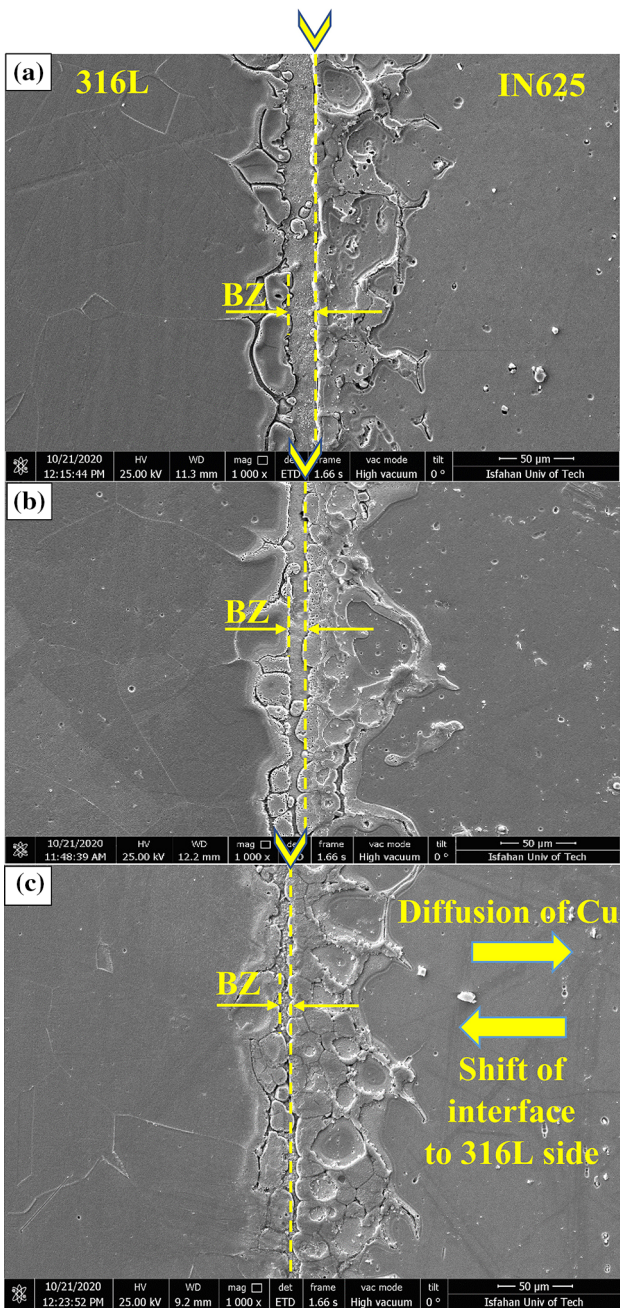


Fig 6. FESEM images of IN 625/Cu/AISI 316L joint made at the bonding temperature of 1100 °C for (a) 15 minutes, (b) 30 minutes and (c) 60 minutes

grain growth occurs. However, at temperatures below 1050 °C, grain growth is slow due to the pinning effects of carbide particles in grain boundaries (Ref 25, 26). Increasing the temperature and time of bonding leads to an increase in the grain size of the base metal. By increasing the grain size, the grain boundary area per unit volume decreases. Hence, the path for the diffusion of Cu to the base metal becomes more limited. A similar trend was observed in the TLP bonding of nickel

metal with the Ni-11wt % P interlayer by Kokawa and Saida (Ref 27, 28).

Figure 9 shows the microstructure of AISI 316L stainless steel base metal in the bonding temperature of 1100 °C with different bonding times. It can be seen that by increasing the bonding time, the grain size of AISI 316L stainless steel has increased and as a result the grain boundary area per unit volume has decreased.

According to Table 4, the width of the DAZ on both sides of the base metals increases with increasing the bonding time. However, the width of the DAZ in 60 minutes due to the increase in grain size has been associated with a smaller increase compared to the bonding times of 15 and 30 minutes.

Figure 10 shows microstructure evaluation model for IN625/Cu/316L TLP bonding. According to Fig. 10(a), Cu melts at the bonding temperature and dissolves the base metal surfaces in contact with molten Cu. With the mutual diffusion of Cu and base metal elements to each other, formation of Mo- and Nb-rich carbides at the interface of Inconel 625 and (Ni, Cr, Fe)-rich intermetallic precipitation in the BZ occurs (Fig. 10b). As the bonding time increases, carbides and intermetallic compounds dissolve in the matrix and the Cu depletion from the BZ ensures that isothermal solidification has occurred (Fig. 10c, d). Due to the diffusion of Cu toward the base metals is not the same and the diffusion of Cu toward Inconel 625 is much more than that of Cu toward 316L stainless steel, so the interface is shifted toward stainless steel (Fig. 6c). The reason for this in terms of thermodynamics and Cu diffusion flux will be explained in the following paragraph.

In IN 625/Cu/AISI 316L joint, diffusion kinetics and diffusion thermodynamics are vital parameters to complete the isothermal solidification (Ref 29, 30). Therefore, there is a competition between diffusion kinetics and diffusion thermodynamics to determine the isothermal solidification rate during TLP bonding. Diffusion kinetics is defined as the permeability of atoms in the base metal. In other words, atoms with higher diffusion coefficients lead to higher atomic fluxes and lower solidification times. The diffusion thermodynamics, expressed in terms of a binary diagram, refers to the difference between the concentrations of Cu atoms in the solid interface (C_S) and the concentration of Cu atoms in the base metal (C_{BM}) and represents the driving force of the diffusion. Because Ni is the predominant element in Inconel 625 alloy and iron is the predominant element in AISI 316L stainless steel, Ni-Cu and Fe-Cu phase diagrams can be useful in finding the thermodynamic parameters. Figure 11 shows the binary diagrams of Cu-Ni and Cu-Fe. The more significant the concentration difference of Cu between the interface (C_S) and the base metal (C_{BM}), the greater the tendency of the Cu atoms to diffusion (i.e., the higher diffusion flux J) and the shorter the isothermal solidification time (Ref 19). According to Fig. 8, the difference between the concentration of Cu in the solid interface (C_S) and the base metal (C_{BM}) in the Ni-Cu diagram ($(C_S)-(C_{BM})_{Cu-Ni}$) is much greater than this difference in the Fe-Cu one ($(C_S)-(C_{BM})_{Cu-Fe}$). Therefore, the driving force for the Cu atoms to diffuse the Inconel 625 base metal will be much greater than that of 316L stainless steel.

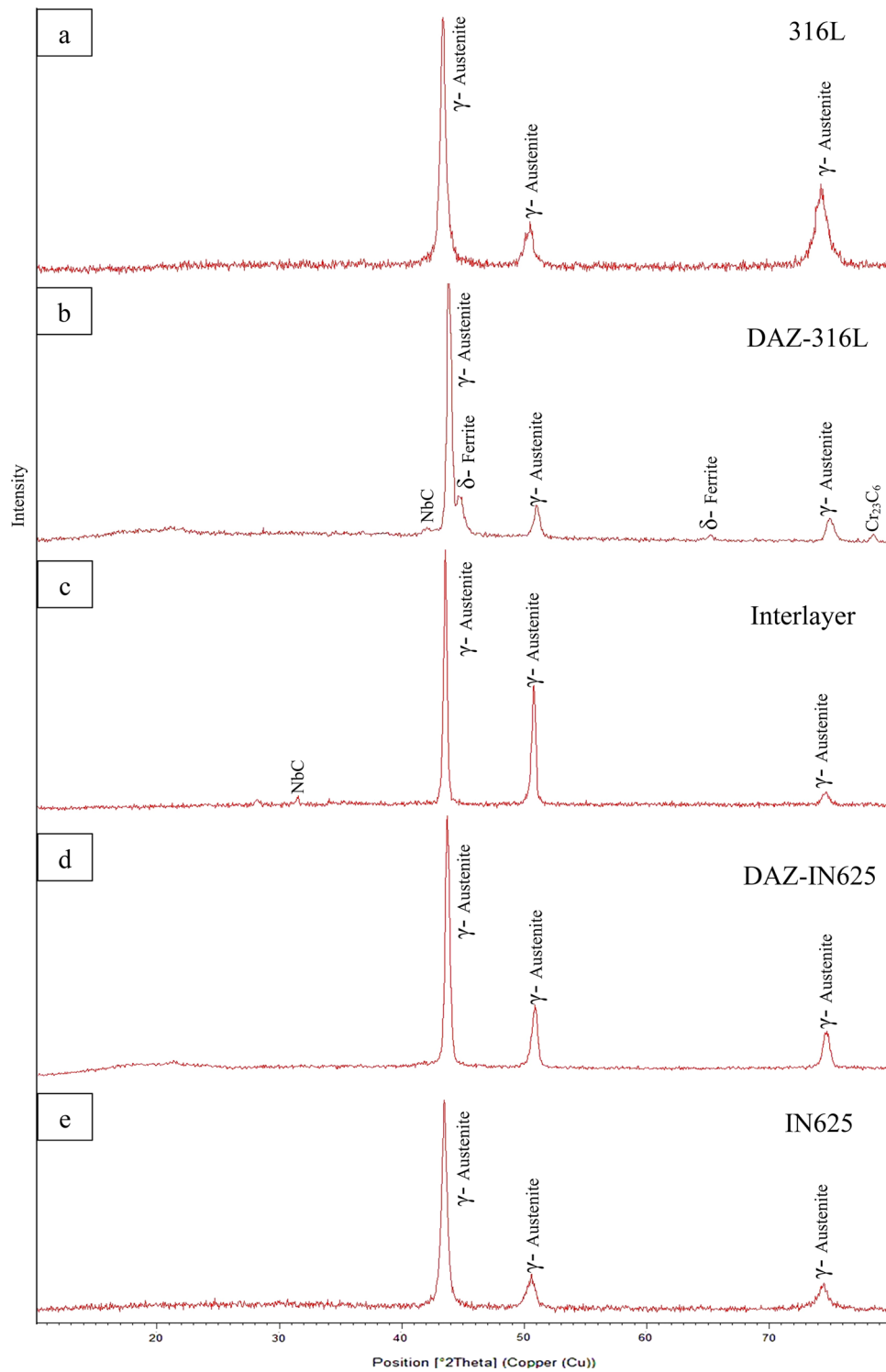
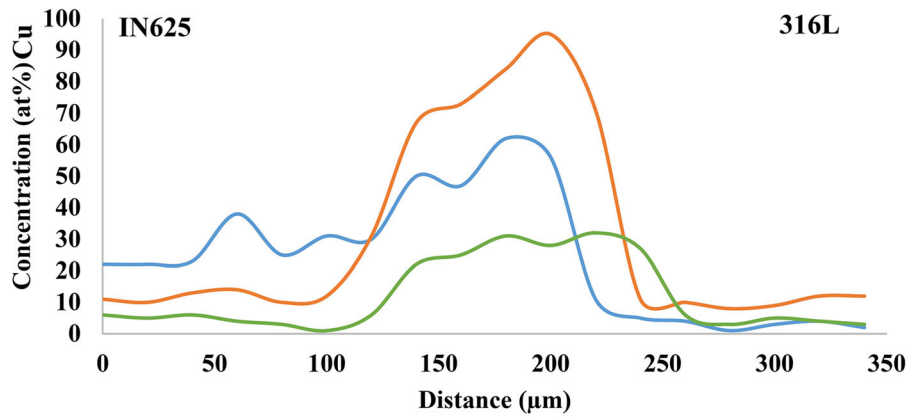
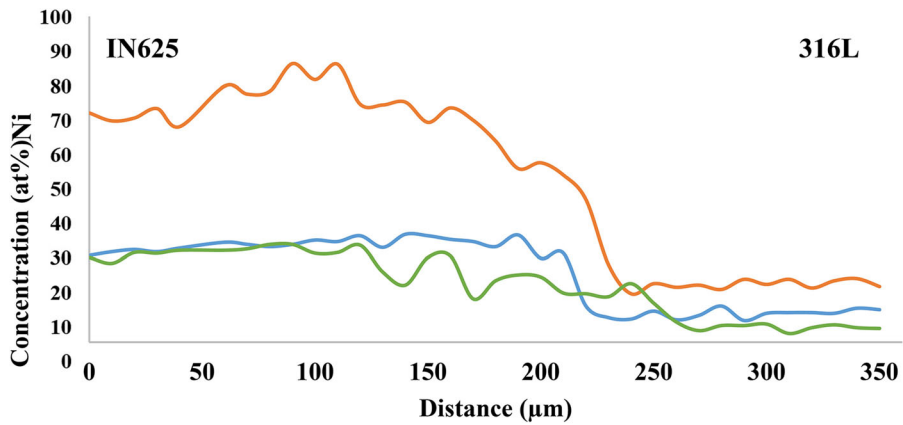


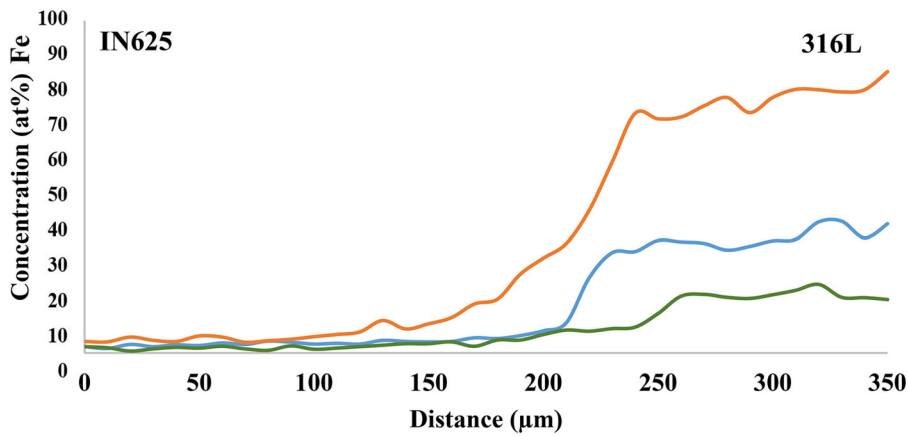
Fig 7. XRD diffraction patterns of (a) 316L BM, (b) DAZ of 316L, (c) interlayer, (d) DAZ of Inconel 625 and (e) Inconel 625 BM



(a) — t=15 min — t= 30 min — t= 60 min



(b) — t=15 min — t=30 min — t=60 min



(c) — t=15 min — t=30 min — t=60 min

Fig 8. Linear EDS analysis across the IN625/Cu/AISI316L joint made at the bonding temperature of 1100 °C for 15, 30 and 60 minutes (a) Cu, (b) Ni and (c) Fe

Table 3 Grain size of 316L stainless steel base metal at different bonding time

Sample	Average grain diameter, μm	ASTM Grain size
As received	13	9.4
1100 °C-15 min	37	6.6
1100 °C-30 min	51	5.9
1100 °C-60 min	89	4.3

Table 5 shows the diffusion kinetics and the diffusion thermodynamics at the temperature of 1100 °C. At the temperature of 1100 °C in the Cu-Ni system, the concentration of Cu in the liquid interface is $C_L^{\text{Cu}} = 95\%$ at. and the concentration of Cu in the solid interface is $C_S^{\text{Cu}} = 93\%$ at. In the Cu-Fe system, the concentration of Cu in the liquid interface is $C_L^{\text{Cu}} = 96.3\%$ at. and the concentration of Cu in the solid interface is $C_S^{\text{Cu}} = 8.5\%$ at. Furthermore, the initial concentration of Cu in base metals is approximately $C_{\text{BM}}^{\text{Cu}} = 0\%$ at.

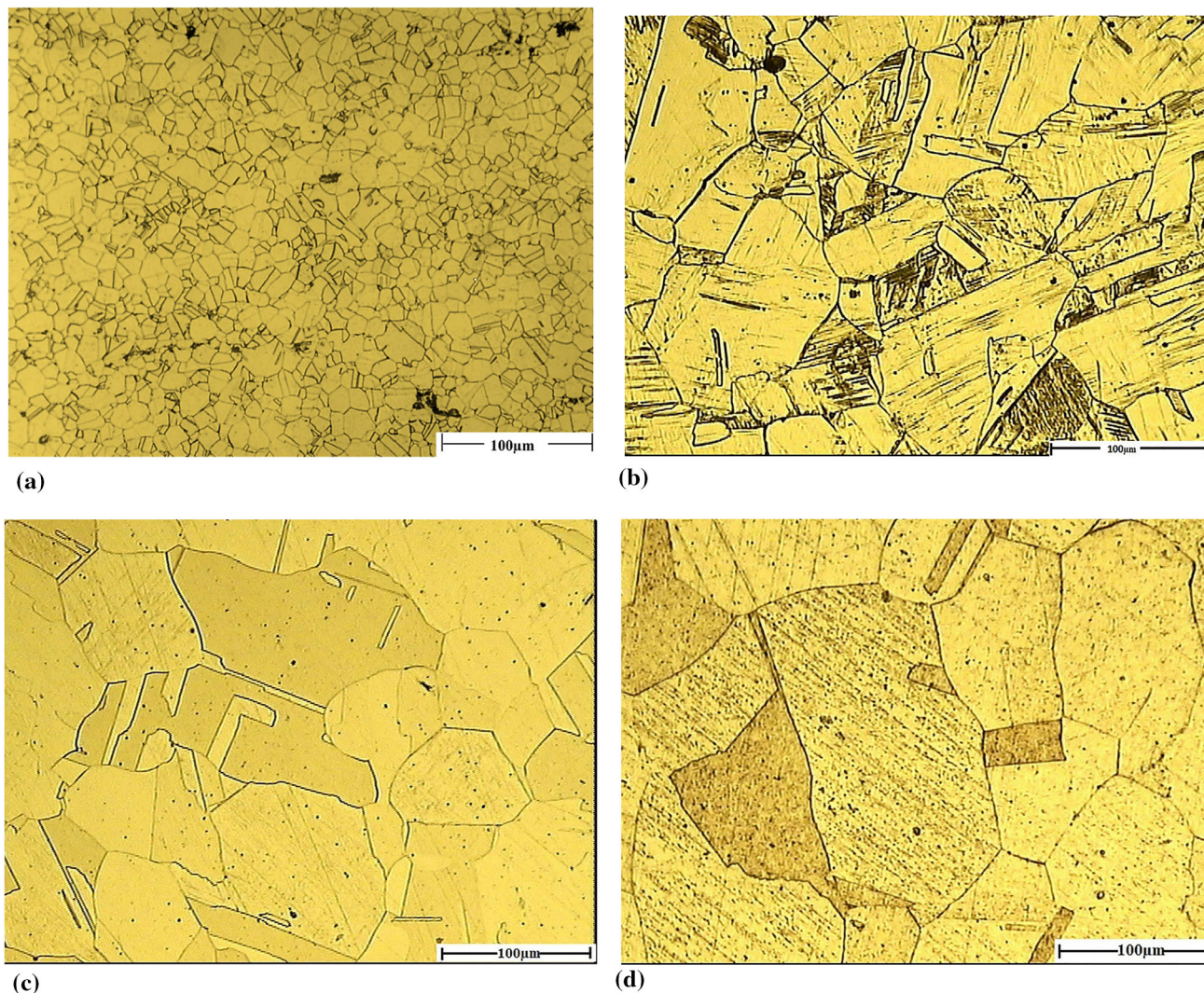


Fig 9. The microstructure of AISI 316L base metal (a) as received and the samples made at the bonding temperature of 1100 °C with the bonding times of (b) 15 minutes, (c) 30 minutes and (d) 60 minutes

Table 4 The effect of time on the width of the BZ and DAZ in IN625/Cu/316L bonding at 1100 °C for times of 15, 30 and 60 minutes

Widths of zones in 1100 °C, μm	15 minutes	30 minutes	60 minutes
BZ	20±5	10±3	1±2
DAZ (316L)	44.24±5	56±6	60±4
DAZ (IN625)	99.64±8	112±7	122±6

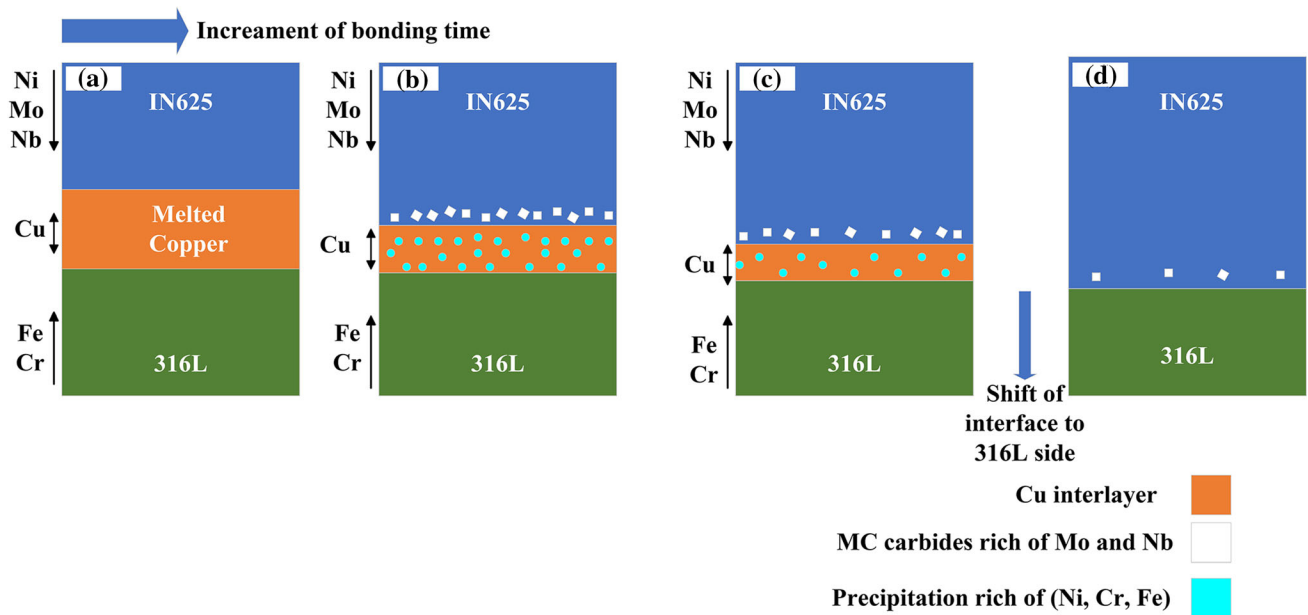


Fig 10. Microstructure evaluation model for IN625/Cu/316L TLP bonding (a) Cu interlayer melting and base metal dissolution, (b) formation of MC carbides rich in Mo and Nb in the Inconel 625 interface and (Ni, Cr, Fe)-rich precipitates in the bonding zone, (c) dissolution of intermetallic compounds and decrease of interlayer thickness with increasing bonding time and (d) end of isothermal solidification and depletion of Cu from BZ

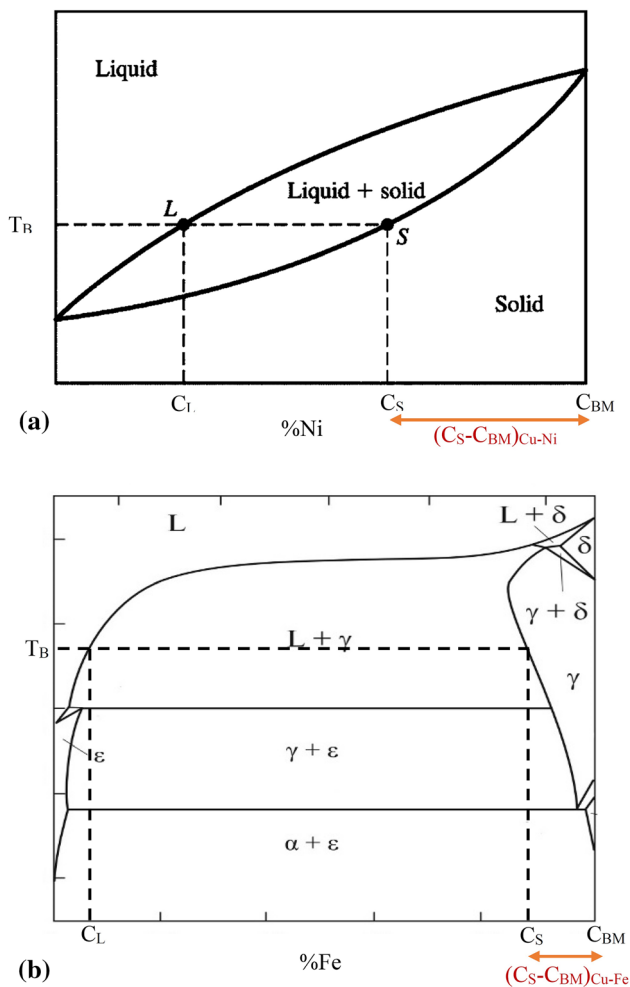


Fig 11. Binary phase diagram of (a) Cu-Ni and (b) Cu-Fe

According to the relation of atomic flux (Eq 1) (Ref 19) with the kinetic and thermodynamic parameters of diffusion and using the values presented in Table 5, the ratio of the flux of Cu atoms in Inconel 625 to the flux of Cu atoms in AISI 316L stainless steel can be calculated according to the following equation:

$$J = -\frac{\sqrt{D_S}}{\sqrt{\pi t}}(C_S - C_{BM}) \quad (\text{Eq 1})$$

$$\frac{J_{\text{Cu} \rightarrow \text{Ni}}}{J_{\text{Cu} \rightarrow \text{Fe}}} = \frac{(C_S^{\text{Cu}} - C_{\text{BM}}^{\text{Cu}})_{\text{Ni}}}{(C_S^{\text{Cu}} - C_{\text{BM}}^{\text{Cu}})_{\text{Fe}}} \times \frac{\sqrt{D_{\text{Cu} \rightarrow \text{Ni}}}}{\sqrt{D_{\text{Cu} \rightarrow \text{Fe}}}} = 30 \quad (\text{Eq 2})$$

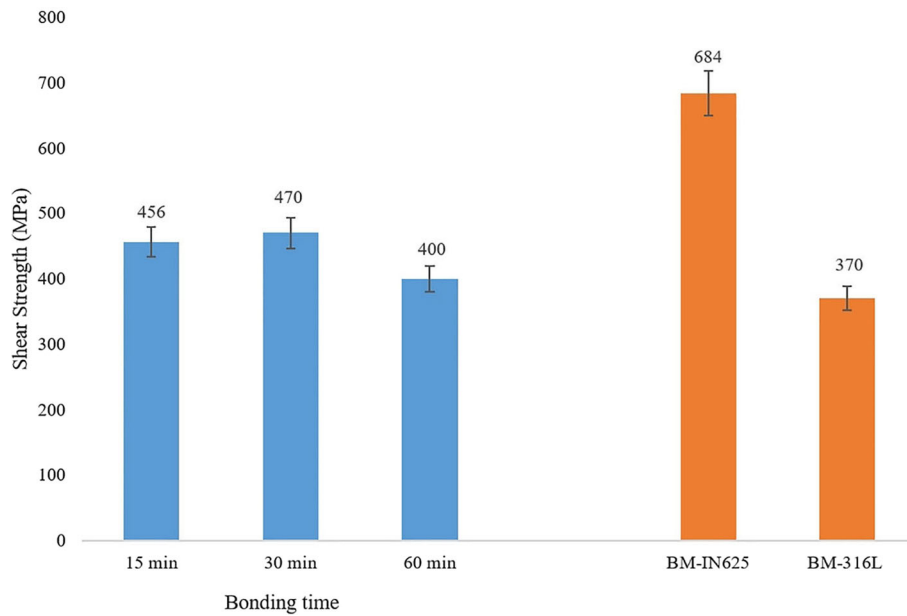
Therefore, the flux of Cu atoms toward Inconel 625 at 1100 °C is 30 times greater than the flux of Cu atoms toward AISI 316L stainless steel.

3.2 Mechanical Properties

Figure 12 shows the shear strength of the joints prepared at the bonding temperature of 1100 °C for bonding times of 15, 30 and 60 minutes compared with the shear strength of base metals. According to Figure 12, the joint made at the bonding temperature of 1100 °C for 30 minutes has the highest shear strength. In the bonding time of 30 minutes, the joints were free of any voids. Therefore, the maximum shear strength was obtained in this bonding time. Increasing the bonding time to more than 30 minutes results in a decrease in shear strength due to the formation of microvoids and coalesces of them in the BZ. Furthermore, with increasing bonding time to 60 minutes results in establishing a complete bonding while micron-sized voids are evident in the BZ, which will significantly affect the bonding quality. Isothermal solidification of molten Cu in the BZ can lead to the formation of solidification shrinkage voids, which reduces the strength of the BZ (Ref 19). Figure 13 shows the microhardness profile of the IN 625/Cu/AISI 316L joint at

Table 5 Isothermal solidification parameters for TLP bonding of IN625/Cu/316L

Bonding system	Diffusion kinetics, Cm^2/S	Diffusion thermodynamics, at. %
Inconel 625-Cu	$D_{\text{Cu} \rightarrow \text{Ni}} = 1.2 \times 10^{-10}$ (Ref 21)	$C_S^{\text{Cu}} - C_{\text{BM}}^{\text{Cu}} = 93$
AISI 316L-Cu	$D_{\text{Cu} \rightarrow \text{Fe}} = 1.16 \times 10^{-11}$ (Ref 20)	$C_S^{\text{Cu}} - C_{\text{BM}}^{\text{Cu}} = 8.5$

**Fig 12.** Shear strength of the samples bonded at 1100 °C for 15, 30 and 60 minutes in comparison with shear strength of base metals

the bonding temperature of 1100 °C for 15, 30 and 60 minutes. As shown in Fig. 13, the maximum hardness of 160 Vickers in the BZ was achieved at a bonding temperature of 1100 °C for 30 minutes. This finding is consistent with the maximum shear strength obtained in joints made at the bonding temperature of 1100 °C for 30 minutes.

The fracture surfaces of both sides of the IN 625/Cu/AISI 316L joints made at the bonding temperature of 1100 °C for 15, 30, and 60 minutes are shown in Fig. 14. As can be seen, the dominant fracture on the stainless steel side is the cleavage fracture (CF) (Fig. 14a) and on the Inconel 625 side is a dimple fracture (D) (Fig. 14b). As the bonding time increases from 15

to 30 minutes the presence of dimples on the 316L (Fig. 14c) and Inconel 625 side (Figure 14(d)) is noticeable, so that the depth of the dimples has increased. Figure 14(e) shows that with increasing the bonding time to 60 minutes the percentage of dimple zones on the 316L and Inconel 625 side has decreased, and cleavage fracture is observed in some areas. The formation of microvoids and their coalesces at the BZ can increase the cleavage fracture and reduce the dimples' depth by increasing the bonding time. Also, increasing grain growth by increasing the binding time can be effective in increasing the formation of cleavage fracture.

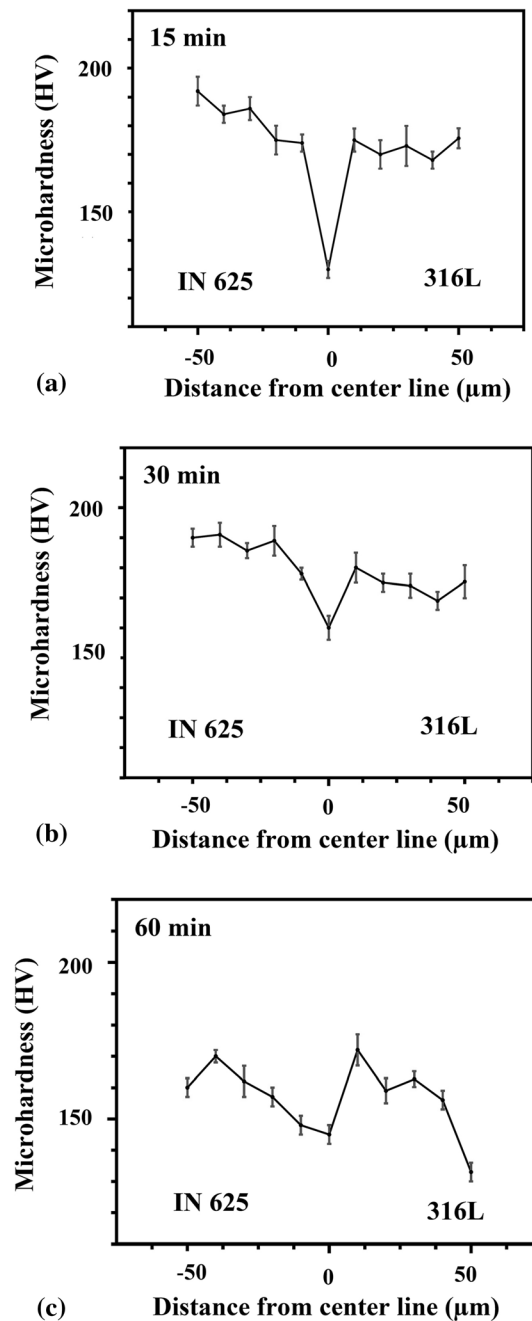


Fig 13. Microhardness profiles in IN 625/Cu/AISI 316L joints made at the bonding temperature of 1100 °C for 15, 30 and 60 minutes

4. Conclusions

In this study, the dissimilar bonding of Inconel 625 to AISI 316L stainless steel was investigated by the TLP bonding method with a Cu interlayer. The main conclusions of this research are as follows:

1. The joint's microstructure at the bonding temperature of 1100°C for 30 minutes indicated that a complete bonding had been established and the bonding is free of any voids.
2. The elemental map analysis taken from the BZ showed that the precipitations formed in the Cu matrix are rich in Ni, Cr, Fe.
3. The linear EDS analysis results from the joint showed that the diffusion of Cu, Ni and Fe is not only a function of the bonding temperature but also depends to some extent on the grain size of the base metals.
4. The shear strength test results showed that the joint made at the bonding temperature of 1100 °C for 30 minutes has the highest shear strength of 470MPa among the performed joints. Furthermore, the microhardness test results indicated that the highest hardness in the BZ was achieved at this temperature and time, which was in accordance with the microstructural results.
5. The formation of microvoids and their coalesces at the BZ can increase the cleavage fracture and reduce the dimples' depth by increasing the bonding time to 60 minutes.
6. Cu diffusion mechanism shows that the bonding of the TLP with the Cu interlayer is controlled by the diffusion kinetics of Cu atoms in the solid-state and the thermodynamics of diffusion.

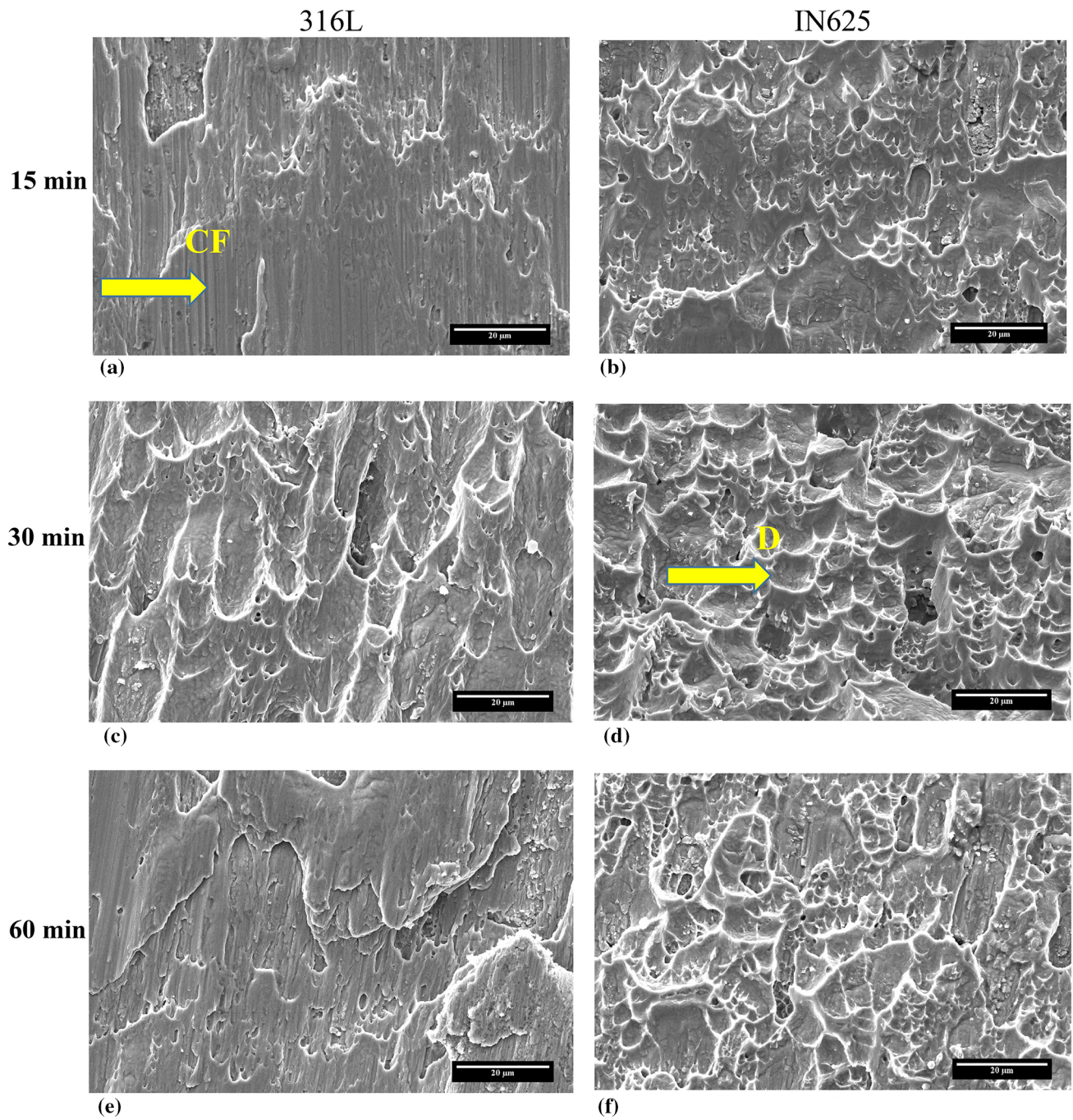


Fig 14. Fracture surfaces of samples made at the bonding temperature of 1100 °C (a, b) for 15 minutes, (c, d) for 30 minutes and (e, f) for 60 minutes

References

1. H.N. Moosavy, M.R. Aboutalebi, S.H. Seyedein and C. Mapelli, A Solidification Model for Prediction of Castability in the Precipitation-Strengthened Nickel-Based Superalloys, *J. Mater. Process. Technol.*, 2013, **213**(11), p 1875–1884.
2. F. Yang, L. Dong, X. Hu, X. Zhou, Z. Xie and F. Fang, Effect of Solution Treatment Temperature upon the Microstructure and Mechanical Properties of Hot Rolled Inconel 625 Alloy, *J. Mater. Sci.*, 2020, **55**(13), p 5613–5626.
3. J. Rodriguez, K. Hofer, A. Haelsig and P. Mayr, Functionally Graded SS 316L to Ni-Based Structures Produced by 3D Plasma Metal Deposition, *J. Met.*, 2019, **9**(6), p 620.
4. P. Mitilesh, D. Varun, A. Reddy, K.D. Ramkumar, N. Arivazhagan and S. Narayanan, Investigations on Dissimilar Weldments of Inconel 625 and AISI 304, *Procedia Eng.*, 2014, **75**, p 66–70.
5. H. Vemanaboina, G. Edison and S. Akella, Weld Bead Temperature and Residual Stresses Evaluations in Multipass Dissimilar Inconel 625 and SS316L by GTAW using IR Thermography and x-ray Diffraction Techniques, *Mater. Res. Express*, 2019, **6**(9), p 0965a9.
6. A. Mishra, D. Dixit and A.K. Sharma, Study on Microstructural and Mechanical Properties of Dissimilar Joint of Laser Beam Welded Inconel 625 and SS 316, *Int. J. Eng. Adv. Technol.*, 2018, **6**(1), p 8–11.
7. L. Romanin, P. Ferro, A. Fabrizi and F. Berto, A Metallurgical and Thermal Analysis of Inconel 625 Electron-Beam Welded Joints, *Frattura ed Integrità Strutturale*, 2019, **13**(50), p 251–263.

8. A. Kourdani and R. Derakhshandeh-haghighi, Evaluating the Properties of Dissimilar Metal Welding Between Inconel 625 and 316L Stainless Steel by Applying Different Welding Methods and Consumables, *Metall. Mater. Trans. A.*, 2018, **49**(4), p 1231–1243.
9. Y.S. Kwon, J.S. Kim, J.S. Moon and M.J. Suk, Transient Liquid Phase Bonding Process using Liquid Phase Sintered Alloy as an Interlayer Material, *J Mater. Sci.*, 2000, **35**, p 1917–1924.
10. V. Maleki, H. Omidvar and M.R. Rahimpour, Effect of Gap Size on Microstructure of Transient Liquid Phase Bonded IN-738LC Superalloy, *Trans. Nonferrous Met. Soc. China*, 2016, **26**, p 437–447.
11. J. Maity, T.K. Pal and R. Maiti, Transient Liquid Phase Diffusion Bonding of 6061–13 vol.% SiCp Composite using Cu Powder Interlayer: Mechanism and Interface Characterization, *J. Mater. Sci.*, 2010, **45**, p 3575–3587.
12. G.O. Cook and C.D. Sorensen, Overview of Transient Liquid Phase and Partial Transient Liquid Phase Bonding, *J. Mater. Sci.*, 2011, **46**, p 5305–5323.
13. B.A. Khazaei, G. Asghari and R. Bakhtiari, TLP Bonding of Dissimilar FSX-414/IN738 System with MBF80 Interlayer: Prediction of Solid/Liquid Interface Location, *Trans. Nonferrous Met. Soc. China*, 2014, **24**, p 996–1003.
14. D. Murraya and S. Corbin, Determining the Kinetics of Transient Liquid Phase Bonding (TLPB) of Inconel 625/BNi-2 Couples using Differential Scanning Calorimetry, *J. Mater. Process. Technol.*, 2017, **248**, p 92–102.
15. Z.P. Liu, G.Y. Zhou, F.Q. Tian, D.Q. Chen and S.T. Tu, Experimental Investigation on the Kinetic Parameters of Diffusion Component for Vacuum Brazing SS316L/BNi-2/SS316L Joint, *Procedia Eng.*, 2015, **130**, p 497–508.
16. M.A. Arafin, M. Medraj, D.P. Turner and P. Bocher, Transient Liquid Phase Bonding of Inconel 718 and Inconel 625 with BNi-2: Modeling and Experimental Investigations, *Mater. Sci. Eng. A.*, 2007, **447**(1–2), p 125–133.
17. A. Doroudi, A. Shamsipur, H. Omidvara and M. Vatanarab, Effect of Transient Liquid Phase Bonding Time on the Microstructure, Isothermal Solidification Completion and the Mechanical Properties during Bonding of Inconel 625 Superalloy using Cr-Si-B-Ni Filler Metal, *J. Manuf. Process.*, 2019, **38**, p 235–243.
18. A. Doroudi, A.E. Pilehrood, M. Mohebinia, A. Dastgheib, A. Rajabi and H. Omidvar, Effect of the Isothermal Solidification Completion on the Mechanical Properties of Inconel 625 Transient Liquid Phase Bond by Changing Bonding Temperature, *J. Mater. Res. Technol.*, 2020, **9**(5), p 10355–10365.
19. W.S. Chen, C.Y. Wang and R.K. Shiue, Brazing Inconel 625 Using the Copper Foil, *Metall. Mater. Trans. A.*, 2013, **44**, p 5724–5731.
20. T. Padrona, T. Khan and M. Kabir, Modelling the Transient Liquid Phase Bonding Behaviour of a Duplex Stainless Steel using Copper Interlayers, *Mater. Sci. Eng. A.*, 2004, **385**(1–2), p 220–228.
21. A. Ghasemi and M. Pouranvari, Fast Isothermal Solidification During Transient Liquid Phase Bonding of a Nickel Alloy Using Pure Copper Filler Metal: Solubility vs Diffusivity, *Metall. Mater. Trans. A.*, 2019, **50**(5), p 2235–2245.
22. W. G. Moffatt, J. H. Westbrook, The Handbook of binary phase diagrams, Schenectady, N.Y.: General Electric Co., Corporate Research and Development Amsterdam, NY: Genium Group, Inc., ©1976
23. S. Ban, Y. Shin, S. Lee and H. Lee, Corrosion Resistance of Inconel 625 Overlay Welded Inside Pipes as a Function of Heat Treatment Temperature, *Int. J. Electrochem. Sci.*, 2016, **11**, p 7764–7774.
24. M. Mohammadi and A. Ekrami, Microstructure and Mechanical Properties of Pure Cu Interlayer TLP Joints of 304 Stainless Steel to Dual Phase Steel, *J. Mater. Process. Technol.*, 2019, **247**, p 116276.
25. M. Liu, W. Jie Zheng, J. Zhong Xiang, Z. Gang Song, E. Xiang Pu and H. Feng, Grain Growth Behavior of Inconel 625 Superalloy, *J. Iron Steel Res. Int.*, 2016, **23**(10), p 1111–1118.
26. J.S. Choi and D.Y. Yoon, The Temperature Dependence of Abnormal Grain Growth and Grain Boundary Faceting in 316L Stainless Steel, *ISIJ Int.*, 2001, **41**(5), p 478–483.
27. H. Kokawa, C.H. Lee and T.H. North, Effect of Grain Boundaries on Isothermal Solidification during Transient Liquid Phase Brazing, *Metall. Mater. Trans. A.*, 1997, **22**(7), p 1627–1631.
28. K. Saida, Y. Zhou and T.H. North, The Influence of Base Metal Grain Size on Isothermal Solidification during Transient Liquid-Phase Brazing of Nickel, *J. Mater. Sci.*, 1993, **28**(23), p 6427–6432.
29. T. Shinmura, K. Ohsasa and T. Narita, Isothermal Solidification Behavior During the Transient Liquid Phase Bonding Process of Nickel Using Binary Filler Metals, *Mater. Trans.*, 2011, **42**(2), p 292–297.
30. T.C. Illingworth, I.O. Golosnoy and T.W. Clyne, Modelling of Transient Liquid Phase Bonding in Binary Systems-A New Parametric Study, *J. Mater. Sci. Eng. A.*, 2007, **445–446**, p 493–500.

Publisher's Note Springer Nature remains neutral with regard to jurisdictional claims in published maps and institutional affiliations.